



Experimental study on shear behaviour of precast shear wall–slab dowel connection

S. Arthi¹ · K. P. Jaya¹

Received: 17 October 2018 / Accepted: 30 January 2020 / Published online: 14 February 2020
© Springer Nature Switzerland AG 2020

Abstract

The primary challenge in any precast structure is its connection between the various elements, mainly the shear wall–slab joint during earthquake. The objective of this study is to predict the shear capacity of the dowel connection under reverse cyclic loading by experimental testing. The study also aims to develop the 3D numerical model for dowel connection between precast shear wall–slab using the finite-element analysis. The performance of the precast dowel connection was measured concerning the failure mode, hysteresis behaviour, ultimate strength, moment carrying capacity, and the ductility factor. The ultimate strength of this dowel connection was 11.17 kN and 11.03 kN in the push and pull direction of loading, respectively. The experimental study was validated with the numerical results and the difference in outcome was found to be only 5%. The model developed was used for the estimation of shear capacity of the connection region. The shear stress developed in the joint region was also found to be within the limit prescribed by various codes.

Keywords Precast dowel connection · Reverse cyclic loading · CDP · Cohesive · Load–displacement curve

Introduction

A precast system consists of various structural members cast in different places and erected to form the final position. The critical issues that occur in a prefabricated system are the response of the connections mainly subjected to seismic loading. Different types of connections are made in prefabricated structures, namely, the wet and dry connection. In case of the wet connection, dowels are provided to take care of the shear acting at the joint region. The design and detailing of connections between the structural and non-structural elements play an important role in resisting the lateral forces arising due to earthquakes (Belleri et al. 2015a, b). The failure of dowel connections in the precast beam–column joint was investigated (Zoubek et al. 2016). Yuksel et al. (2015) studied the seismic performance of two types of exterior precast beam–column connection with and without the presence of corbel. In this type of connection,

half of the beam were precast, and after placing the longitudinal reinforcement that connects the stirrups provided in the precast beam, the screed concreting was done. Rahman et al. (2006) investigated the behaviour of four types of precast beam–column connections. In type 1, the dowel bars projecting the corbel in the precast column were inserted into the sleeve hole provided in the precast beam and the gap was filled with non-shrink grout. In type 2, the dowel bars were bolted through the top angle cleat, and the angle cleat got connected to the precast column using threaded bolts. In type 3, the angle cleat was stiffened with two side plates. In type 4, with the stiffened angle cleat, two threaded bolts were inserted into the column. Soudki et al. (1996) carried out the experimentation on horizontal connections for precast wall panels. The connection between the two precast wall panels was made using mild steel reinforcement, post-tensioning, and shear keys.

Brunesi et al. (2015) investigated the seismic performance of the precast RC-framed structure. In this study, a three-fourth-scaled three-storey-framed structure was tested under displacement-controlled cyclic loading. The incompatible transfer of lateral load and displacement lead to less ductility and failure of the connections. Casotto et al. (2015) developed the methodology for fragility assessment of the precast reinforced concrete structures subjected to ground

✉ S. Arthi
arthisubramanian.s@gmail.com

K. P. Jaya
kpjaya@nayan.co.in; jayakp@annauniv.edu

¹ Department of Civil Engineering, Anna University, Chennai, India

motions considering the beam–column failure mechanisms. Beilic et al. (2017) developed a fragility model for RC precast structure using two different non-linear seismic analysis. It was observed that the connection between the beam and column forms the weakest line, that is not able to transfer the lateral forces in to the column. The developed model exactly predicted the connection in the beam–column failure. Belleri et al. (2015a, b) investigated the seismic performance and proposed the retrofitting techniques for precast industrial structures consisting RC columns with socket foundation and prestressed RC roofs. The failure of the structure under seismic loading was due to the loss of support at the connection, inadequate diaphragm action, limited ductility of columns, and the out-of-plane failure of masonry walls. The structure was retrofitted by providing friction connections using mechanical devices to improve the structural behaviour under seismic loading. The connection between the precast wall panels using loop connection and steel channels connected by nuts and screws were investigated by Taheri et al. (2016).

Brunesi and Nascimbene (2017) experimentally and numerically investigated the seismic response of precast concrete shear walls to foundation and wall-to-wall connections subjected to cyclic loading. In wall-to-wall connections, the hook reinforcement was fastened to the external longitudinal reinforcement using threaded bolts and steel plates. The wall-to-foundation connection was done by starter rebars. The authors concluded that the wall-to-wall connections form the weakest link and the failure was due to the shear. The sliding response seen at the base of the wall was due to the shear-buckling failure of the threaded anchor rods.

Belleri et al. (2017) investigated the performance of two mechanical devices used at the precast hinged beam-to-column joint for energy dissipation and to reduce lateral deformations. The energy dissipation (ED) device increased the hysteretic damping of the system and the stiffening/re-centring (SR) device increased the stiffness of the connection.

The seismic performance of the RC single storey precast structure designed as per the Italian code was assessed by means of nonlinear dynamic and static analysis with respect to the limited state of collapse by Ercolino et al. (2018). The authors concluded that the capacity of the structure was influenced by the seismic conditions and the structural over strength. The full scale two-storey precast RC wall–slab structure subjected to cyclic loading was tested experimentally by Brunesi et al. (2018). The slab was connected to the wall using the layer of fabric-felt material. The authors concluded that the wall–slab joint formed the weakest link and was failed by flexure and crushing of grout at the joint region. The tested specimen was retrofitted by providing steel angles at the wall–slab joint to increase the lateral load resistance of the connection.

The numerical modelling of precast beam–column dowel connection was done using the finite-element software, ABAQUS to simulate the seismic response of the connection. The dowels embedded in the column were inserted into the housing provided in the beam, and then the gap is filled with mortar (Magliulo et al. 2014; Kremmyda et al. 2013). It is crucial to define the models for the materials used and the interaction between the precast connections (Zoubek et al. 2014). The interface shear strength is significant for the modelling of concrete surfaces cast at different times (Mohammad et al. 2015; Papanikolaou and Thermou 2015). Some authors explain the capability and the consecutive theory of the CDP model which realistically captures the response of the structures (Alfarah et al. 2017). In this present work, the concrete damaged plasticity model was used for modelling the non-linear properties of the concrete. Literature works are available on modelling the dowel connections between precast beam–column, column–foundation, wall–wall etc. However, the works related to precast shear wall–slab dowel connection is minimal.

Significance of the study

In spite of sufficient literature available on the seismic behaviour of precast connections, the existing database on the tested precast shear wall–slab dowel connection subjected to reverse cyclic loading are still scarce and it needs particular importance since it forms the weakest section in structures during earthquake. The authors aim to develop a ductile precast shear wall–slab dowel connection and present a 3D numerical model which accurately predicts the shear behaviour of the precast dowel connection subjected to reverse cyclic loading.

Experimental investigation

Design criteria

The test specimen was representative of an exterior shear wall–slab connection in the bottom storey of an eight-storey building located in Chennai and was designed for all the loads transferred from the above stories. The critical design forces obtained from the Staad pro analysis such as the bending moment, shear force and the axial load were 2520.48 kNm, 963.04 kN and 1757.11 kN, respectively. The design and detailing of the shear wall and the slab were done as per IS 456-2000 and IS 13920-1993, respectively. The reinforcement and connection detailing are shown in Fig. 1. The specimen was cast for one-third scaled model. The test specimen comprised of (a) the ground floor shear wall (b) the ground

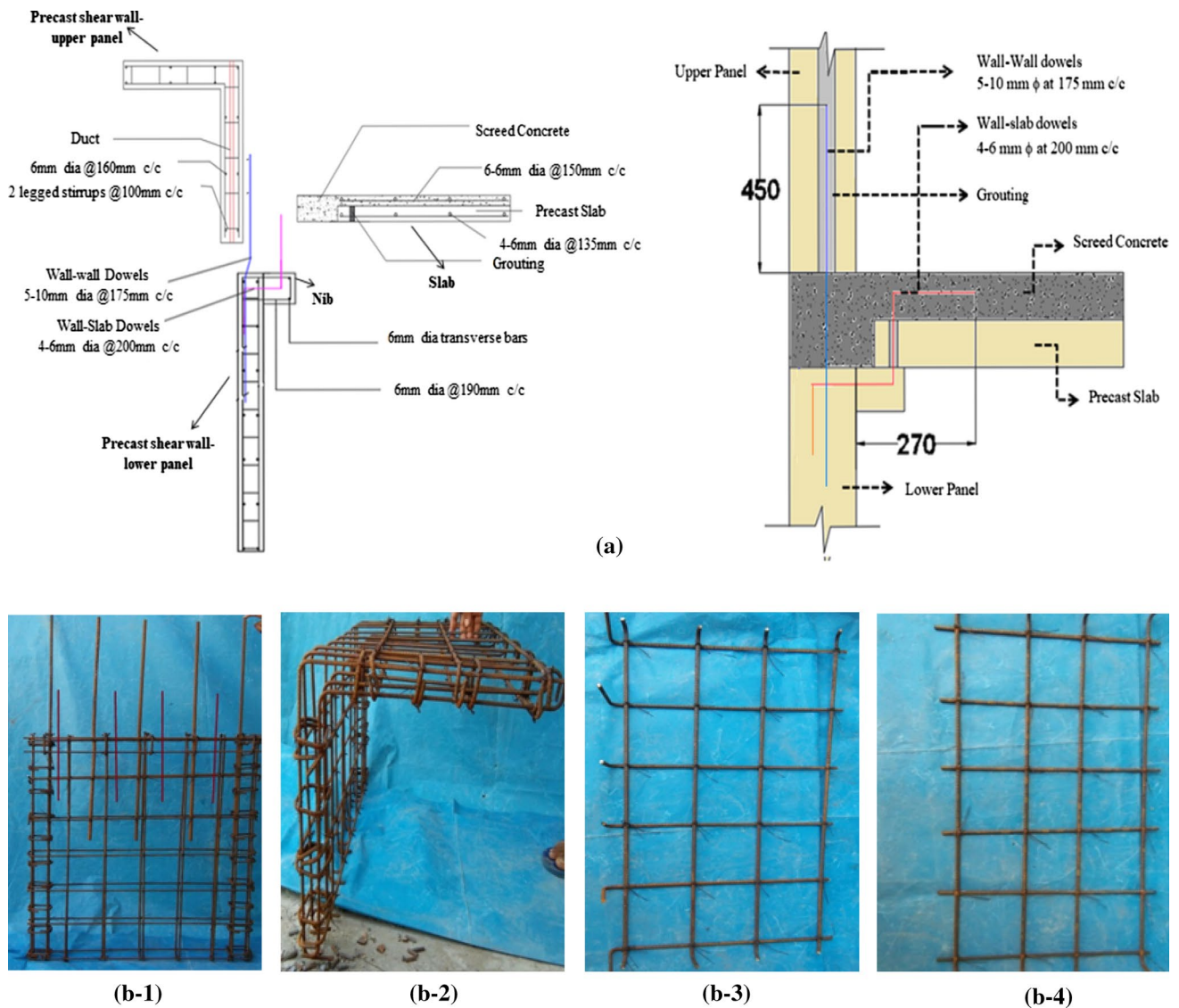


Fig. 1 a Reinforcement and connection detailing. b Bar bending schedule (b-1) Precast shear wall-lower panel (b-2) Precast shear wall-upper panel (b-3) Precast slab (b-4) Screed reinforcement

floor roof slab (c) the first-floor shear wall up to a mid-height. The dimensions of the shear wall-lower panel and upper panel were 800 mm \times 1000 mm \times 80 mm and 800 mm \times 500 mm \times 80 mm, respectively. The upper wall was provided with the projecting slab cast monolithically for the application of axial load. The dimensions of the precast slab and screed concrete were 800 mm \times 430 mm \times 30 mm and 800 mm \times 430 mm \times 30 mm, respectively. The screed concrete was done to maintain the diaphragm action of the slab. The dowel was designed based on the shear force acting on the joint from the slab (Elliot 2017). M30 grade of concrete and Fe 500 grade of HYSD bars were used for

casting the specimen. The average compressive strength of the concrete was 39.2 N/mm².

Assembly of the precast specimen

The precast specimen consists of three parts namely, the shear wall with a nib-lower panel, an upper panel, and the precast slab with screed concrete. Four 6 mm diameter bars with a development length of 270 mm were used for the connection between the precast shear wall lower panel and the precast slab. The precast slab was provided with housing for inserting the dowel bars projecting from the lower panel. The gap between the dowel bars and the duct was filled with high-strength M60 grade grout. The upper

Table 1 Assembly sequence of the precast specimen

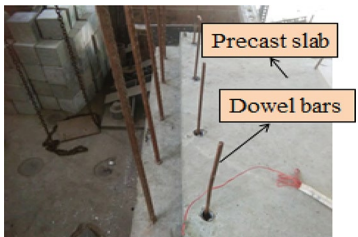

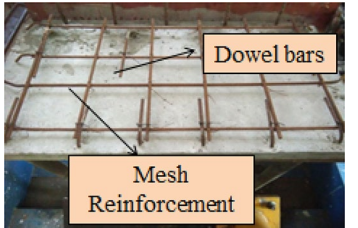
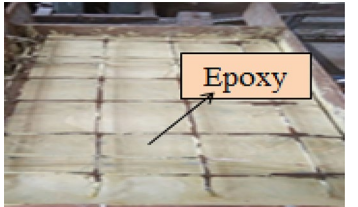


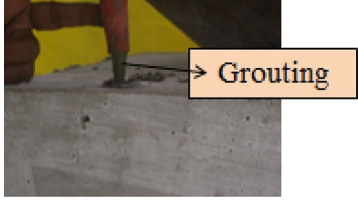
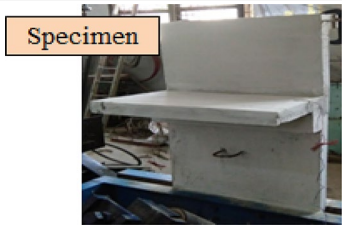
S. no.	Assembly sequence	Figures
1	The shear wall-lower panel was fixed in the frame The precast slab was placed and the dowels were inserted into the housing provided in the precast slab	 <p>Precast slab Dowel bars</p>
2	Grouting was done for filling the gap between dowels and duct provided in the precast slab	 <p>Grouting</p>
3	Mesh reinforcement was placed above the precast slab Dowels were bent and tied with the mesh reinforcement	 <p>Dowel bars Mesh Reinforcement</p>
4	Epoxy was applied before casting the screed concrete for the proper bonding between the concrete cast at different times	 <p>Epoxy</p>
5	Screed concreting was done and then cured	 <p>Screed Concreting</p>
6	Dowels protruding from the shear wall-lower panel were inserted into the housing provided in the shear wall-upper panel The shear wall-upper panel was erected	 <p>Upper Panel Dowel bars</p>
7	Grouting was done to fill the gap between dowels and duct provided in the shear wall-upper panel	 <p>Grouting</p>

Table 1 (continued)

S. no.	Assembly sequence	Figures
8	The final erected stage of the specimen	

panel was also provided with the duct to create housing for inserting the dowel bars protruding from the lower panel. The sequence of assembling the precast specimen is shown in Table 1.

Test set up and procedure

Due to lateral loading, the shear wall–slab joint is subjected to the in-plane moment at the joint region. The couple of

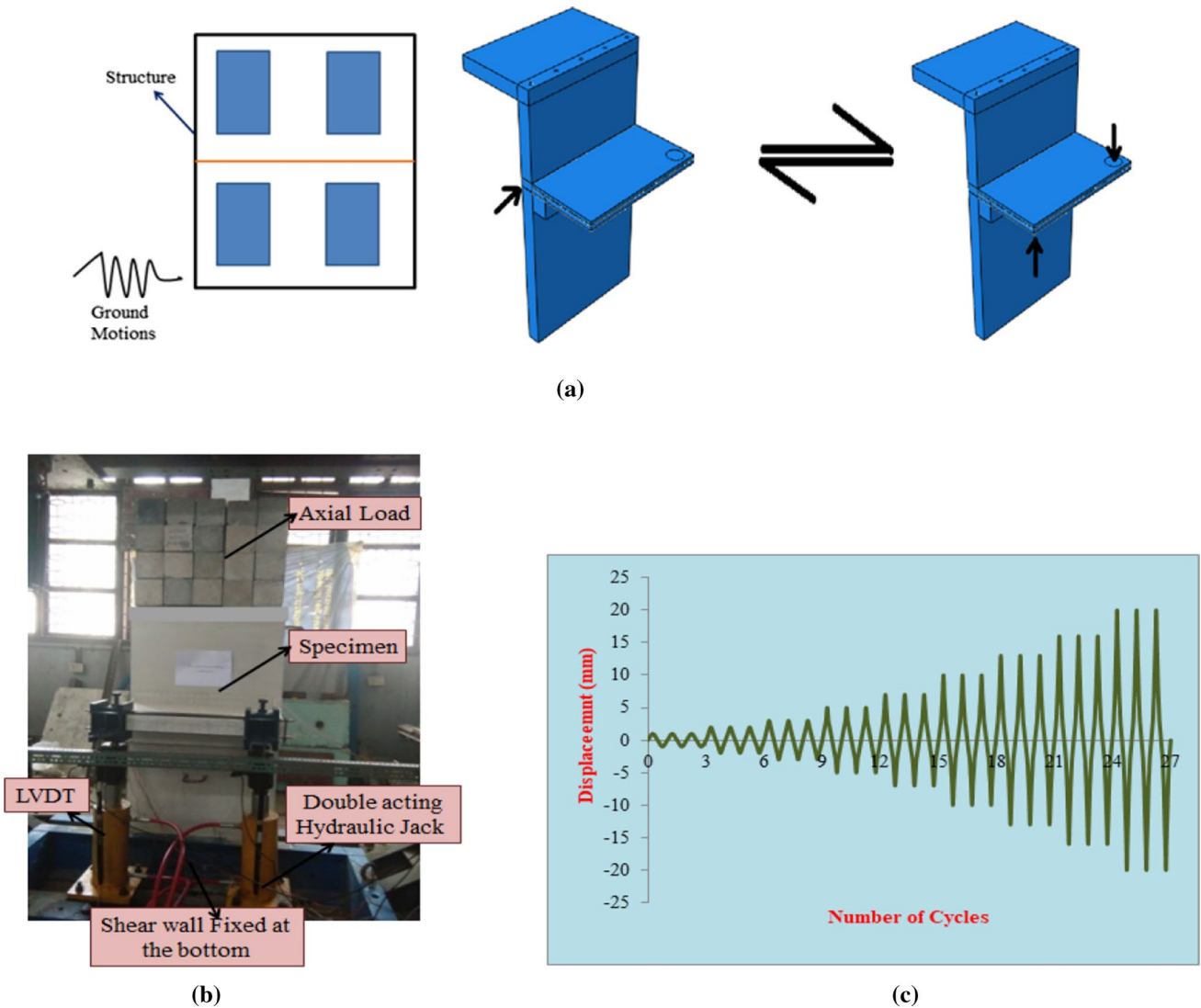


Fig. 2 a Simulation of reverse cyclic loading b Test set up c Loading protocol

forces acting at the slab ends have simulated the in-plane moment as shown in Fig. 2a. The shear wall was fixed at the base using high-strength threaded rods to the frame fixed in the strong floor. Two numbers of double acting jacks were used for the application of reverse cyclic loading at the slab ends as shown in Fig. 2b. The reverse cyclic loading was simulated by applying a push (positive) and pull (negative) direction loading at the slab ends. The concrete cubes were arranged at the top of the projecting slab for the application of the axial load. Two load cells and LVDT was used to measure the load and the displacement, respectively. The displacement-controlled loading concept was used in this study. Each displacement level was applied three times and the loading history is shown in Fig. 2c.

Numerical study

The finite-element analysis of the exterior precast shear wall–slab dowel connection was done using the ABAQUS software. One-third of the scaled-down model was done and the analysis was performed for the reverse cyclic loading similar to the experimental test program.

Modelling

In this study, the concrete (Shear wall, slab) and the grout elements were modelled using a 3D deformable element selected from the ABAQUS three-dimensional solid element library. The assigned solid section was meshed using

C3D8R (Zoubek et al. 2014) element with hour-glass control. The reduced integration element was chosen because it uses a lower order integration to form the element matrices and reduces the running time, especially in three dimensions (Nascimbene 2014). The steel bars were modelled using the 3D 2-noded linear beam element (B31) (Surumi et al. 2015) with the circular profile of 6 mm diameter. An 8-noded three-dimensional cohesive element COH3D8 of thickness 1 mm was used to define the interaction between the structural members such as the shear wall lower panel and the precast slab. The parts such as shear wall—lower panel, upper panel—the precast slab with screed concrete, and the reinforcements were modelled as shown in Fig. 3a, b. The global mesh sizes of the concrete and the reinforcement were 50 and 40, respectively.

Material properties

In this non-linear analysis, the concrete damage plasticity (CDP) was used to model the concrete properties which exactly predicts the inelastic response of the material under reverse cyclic loading (Dere and Koroglu 2017). The CDP model included two failure mechanisms namely crushing (compression) and cracking (tension) of concrete. The main challenge in the CDP model is to define the damage parameter for both compression and tension. The methodology used for calculating the compression and tension behaviour and the damage variables were according to the study carried out by Alfarah et al. (2017). The damage parameter was defined to a maximum of 0.9. The elastic properties of concrete,

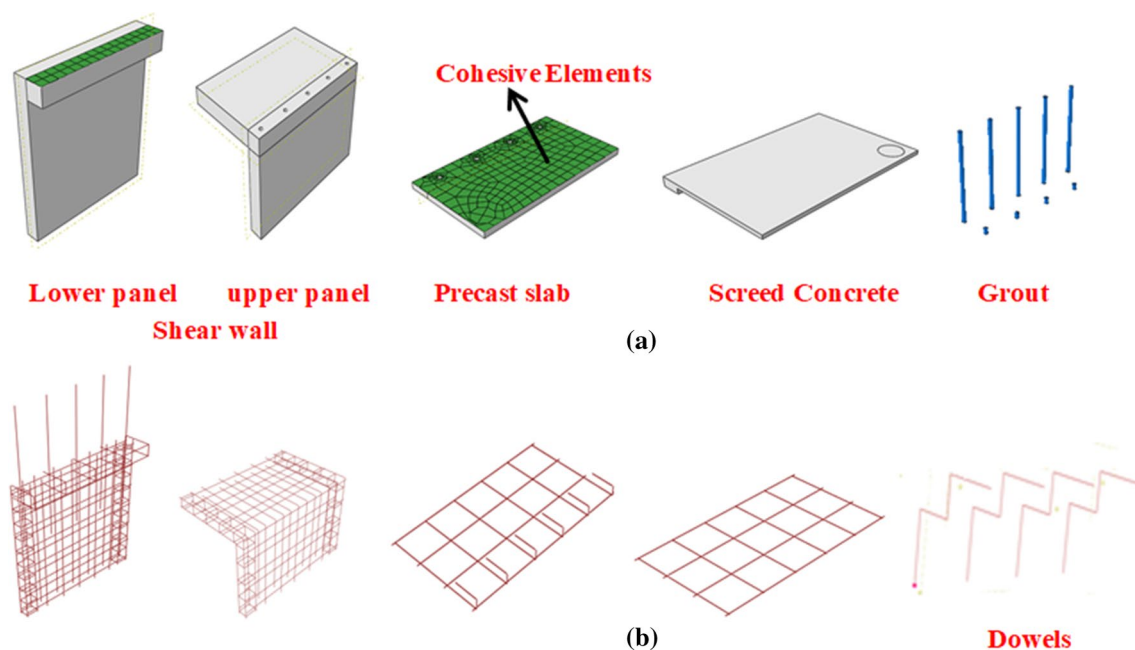


Fig. 3 Modelling in ABAQUS **a** concrete parts **b** reinforcement

Table 2 Elastic properties of concrete, grout and steel

S. no.	Part	Elastic modulus (N/mm ²)	Poisson ratio
1	Concrete	32,725.49	0.2
2	Grout	32,000	0.2
3	Steel	200,000	0.3

Table 3 Plastic properties in CDP model

S. no.	Description	Value
1	Dilation angle	38
2	Eccentricity	0.1
3	Initial/biaxial stress ratio	1.12
4	<i>K</i>	0.67
5	Viscosity parameter	0.666

Table 4 Compression and tension behaviour in CDP model

Compression behaviour			Tension behaviour		
Inelastic strain	Yield stress (N/mm ²)	dc	Cracking strain	Yield stress (N/mm ²)	dt
0	16.36	0	0.00000	3.47	0
0.0007	35.31	0	0.00014	2.63	0.14
0.0013	44.92	0	0.00064	1.57	0.52
0.0017	47.00	0	0.00114	1.04	0.75
0.01	25.69	0.5	0.00139	0.88	0.82
0.0195	8.83	0.8	0.00189	0.68	0.91
0.0295	4.07	0.96	0.00239	0.55	0.96

grout and the steel was given in Table 2. The plastic properties related to dilation angle, eccentricity, initial to biaxial ratio, *k*, viscosity parameter and damage in compression and

tension behaviour are defined in the CDP model and was tabulated in Tables 3 and 4. The plastic phase of steel was modelled using the bilinear behaviour including yield stress and plastic strain.

Interaction, boundary conditions and loading protocol

In this study, the embedded region constraint (Fig. 4a) was used for the interaction between concrete (host region) and reinforcement/dowels (embedded region), since there is no slip between dowels in the connection region. The tie constraint was used between the screed concrete and the upper panel shear wall since there is no separation observed during the testing in the laboratory.

To define the constitute response of the cohesive element in terms of traction versus separation, the traction-separation law was chosen to define the section behaviour of the cohesive element as shown in Fig. 4b. This law assumes initially the linear elastic behaviour followed by the initiation and evolution of damage (ABAQUS 2012). The damage initiation and evolution between the precast slab-screed concrete interfaces and the shear wall lower panel-precast slab interfaces were defined by stiffness ($K_0 = 398.28 \text{ N/mm}$) and the fracture energy along normal shear direction was 90 J/m^2 , first and second shear directions were about 900 J/m^2 (obaidat et al. 2010; Fib 2012).

The boundary conditions were applied similar to the experimental test. A fixed support was assigned to the base of the shear wall. The axial load was distributed as pressure at the projecting slab provided at the top of the upper panel. The displacement-controlled loading was input as a smooth step amplitude function and was applied at the circular shape partition created at the ends of the slab. The analysis was carried out in two steps such as the axial load defined in the first step and the cyclic load was applied in the second step (Fig. 4c, d).

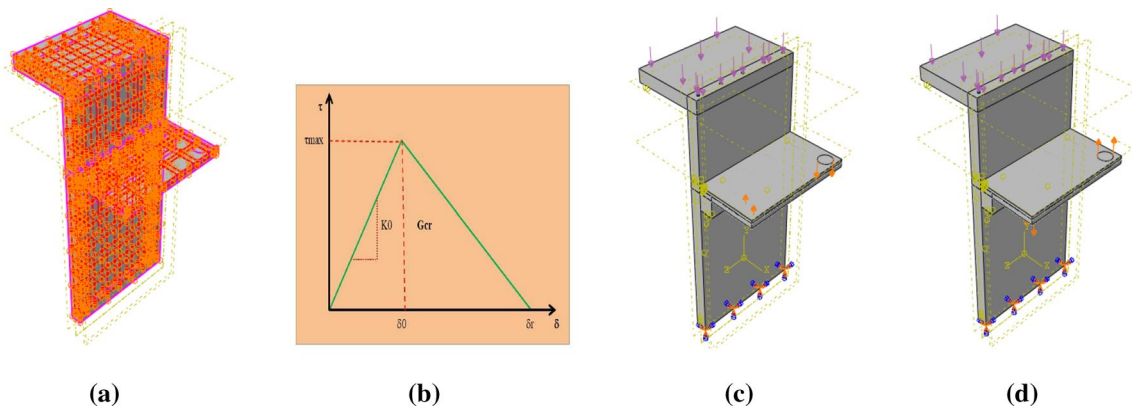


Fig. 4 a Interaction–embedded constraint b Traction–separation constitutive law c Push direction loading d Pull direction loading

Results

The experimental and finite-element analysis results were represented by the key parameters such as ultimate strength, displacement, load–displacement graph, ultimate moment, ductility ratio, and cracking pattern.

Visualization

Failure mode—experimental testing

The crack in the specimen opened and closed on reverse cyclic loading. The crushing and spalling of concrete were observed at the slab ends near the loading region. There was no visible crack found in the shear wall. In this precast specimen, the initial crack was observed at 2 mm (8.48 kN) and the crack started to extend when displacement increased. The shear crack occurred diagonally from the loading point towards the joint region at both the ends of the slab. The crack pattern is shown in Fig. 5a. The debonding between the precast slab and screed concrete was seen at 5 mm positive displacement cycle (11.17 kN) (Fig. 5b). The crack widened at the shear wall with the nib—precast slab junction at 10 mm negative displacement (9.07 kN).

Finite element analysis (FEA)

The concrete damage plasticity model exactly predicted the non-linear behaviour of concrete both in compression and tension. This numerical model accurately simulated the performance of precast dowel connection when compared with the experimental results and these were visualized by the outputs such as crack pattern at joint region, the compressive and tensile damage, and the von-mises stress. Figure 6 shows the FEA results such as compression and tension damage,

principal strain, and the von-mises stress of the exterior precast shear wall–slab dowel connection.

- (a) *Failure mode and principal strain* From Fig. 6a–c, it was observed that as the displacement increases, the damage in the slab increases and the developed model exactly predicted failure mode of the specimen as similar to the test results. The maximum plastic principal strain visualizes the initiation of crack in the CDP model.
- (b) *Von-mises stress* In this study, the steel is modelled as an elastic–plastic material. Therefore, the stress in reinforcement (steel) of the specimen was monitored through the Von-mises stress criteria. As displacement increased, there was continuous increase in strain in all reinforcement bars. The strain measured in longitudinal reinforcement of the slab was found to be higher than the strain in the dowel bars placed at the joint region for precast specimen which showed the slab failure mode.
- (c) *Deformation* The push and pull direction loading was applied at the slab ends in Y-direction. Therefore, the displacement of the specimen was monitored through deformation (U2) in Y-direction. The displacement corresponding to ultimate load of the specimen in the push and pull direction is shown in Fig. 7.

Hysteresis behaviour

The specimen was subjected to reverse cyclic loading. Each displacement was applied three times and the average load vs the displacement curve was plotted from both the experimental and FEA results as shown in Fig. 8. Figure 8a shows a wider hysteresis curve and also the pinching effect due to the reverse cyclic loading. It was also observed that as

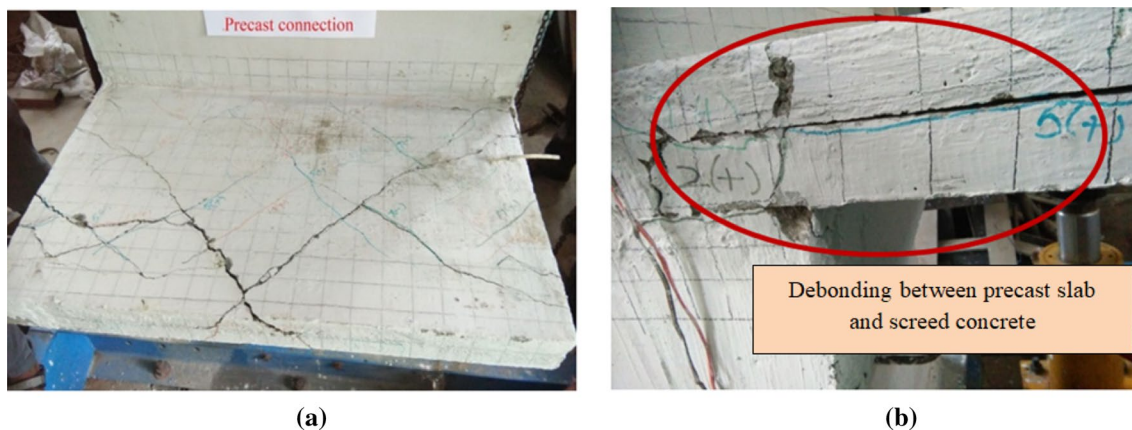


Fig. 5 a Failure mode of the specimen b Crack at the joint region

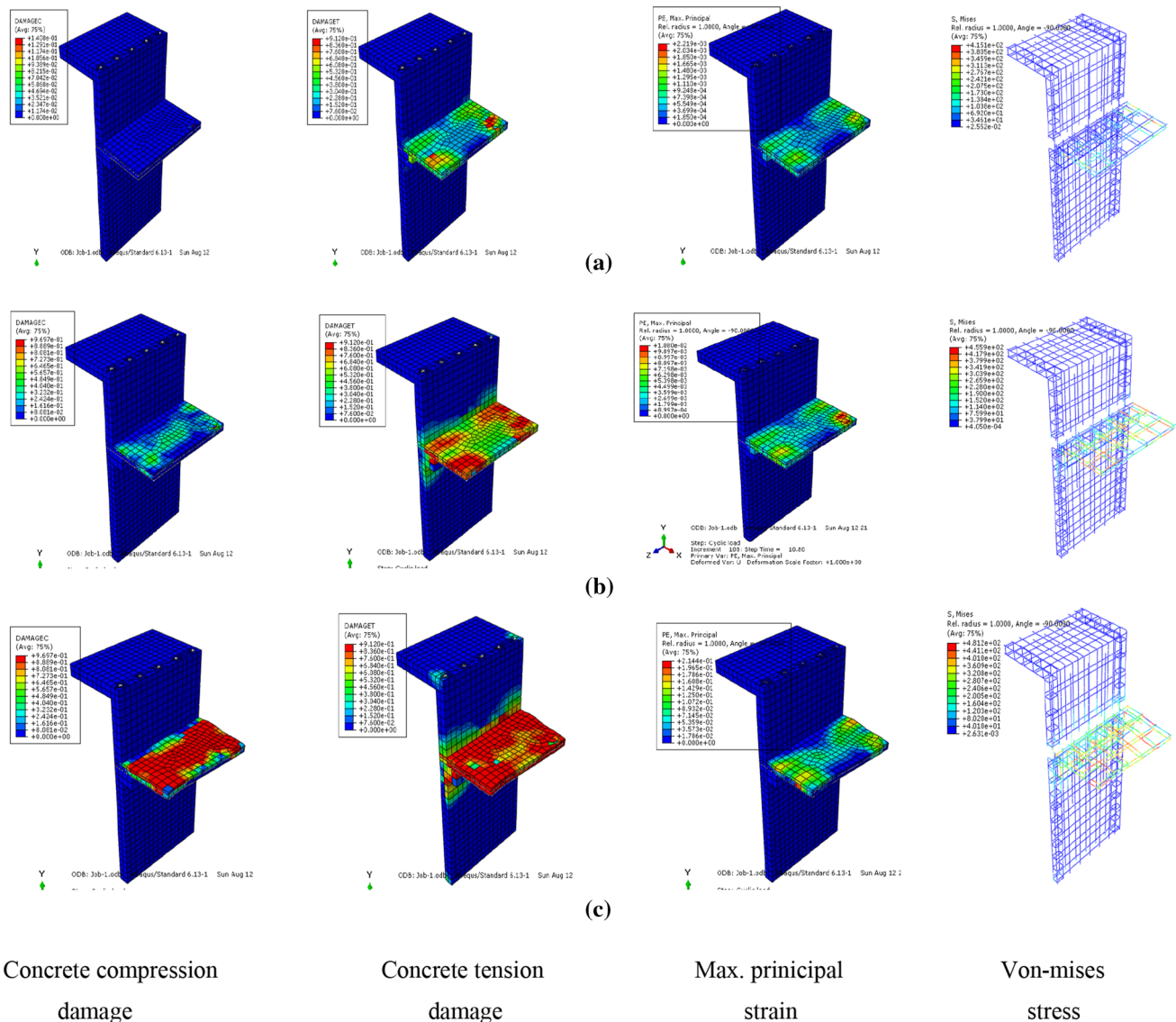


Fig. 6 Visualisation at **a** 2 mm displacement **b** 5 mm displacement **c** 20 mm displacement

displacement increased, the area under the hysteresis loop for each loading cycle increased which showed good energy dissipation capacity of the specimen. The ultimate load carrying capacity of the precast specimen reached at 5 mm displacement. The load carrying capacity of the specimen showed a dropping trend beyond 5 mm and almost became stable until the failure of the specimen. The maximum displacement reached by the precast specimen was 20 mm. The developed model accurately predicted the cyclic shear behaviour, and the capacity of the dowel connection as same as the experimental results. The envelope curve was shown in Fig. 8d. The difference in FEA results of the ultimate load was only 5% when compared with the experimental result which was acceptable.

Ultimate load

The comparison of ultimate load carrying capacity from experimental and finite element analysis result is shown in Fig. 9. The ultimate strength of this dowel connection obtained from the experimental test was 11.17 kN and 11.03 kN in the push (positive) and pull (negative) direction, respectively. The ultimate load from the finite element analysis was found to be 11.68 kN and 11.55 kN in the push and pull direction, respectively. The difference in the ultimate load carrying capacity obtained by the finite-element analysis as compared with the experimental result was found to be 4.6%.

Fig. 7 Deformation at ultimate load **a** Push direction **b** Pull direction

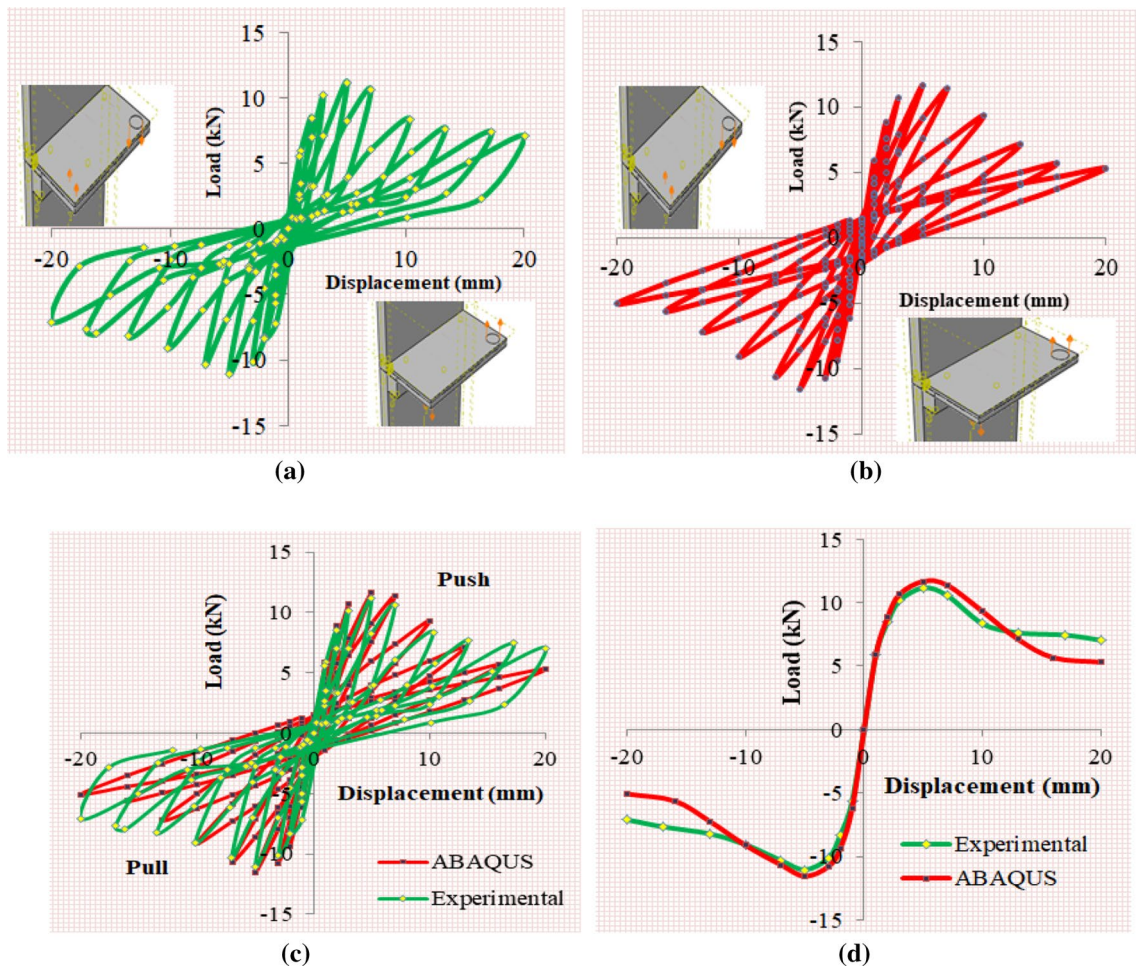
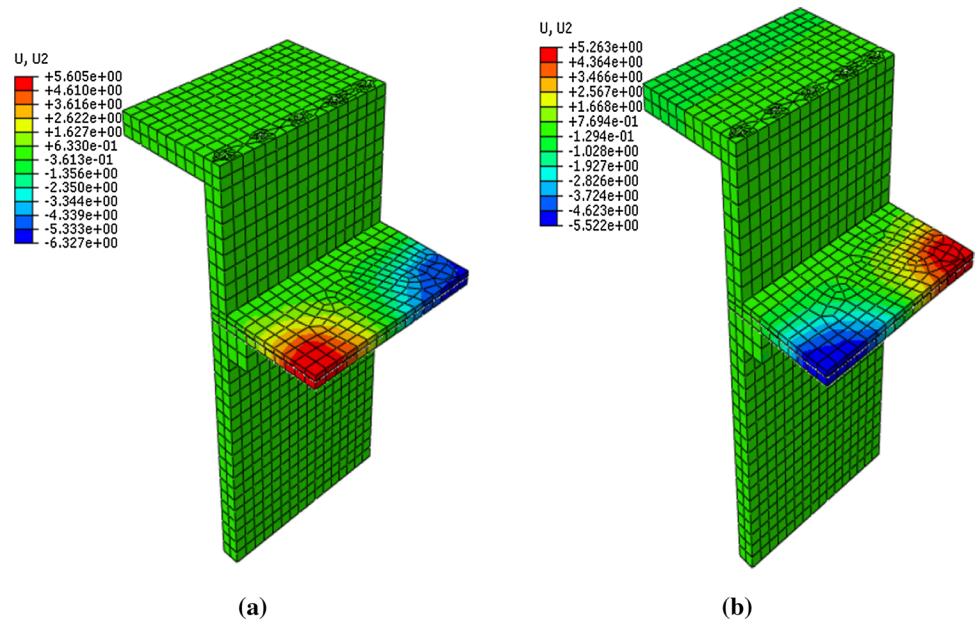


Fig. 8 Load–displacement curve **a** Experimental result **b** FEA result **c** Comparison graph **d** Comparison of load envelope curve

Fig. 9 Comparison of ultimate load carrying capacity from experimental and FEA **a** Positive direction **b** Negative direction

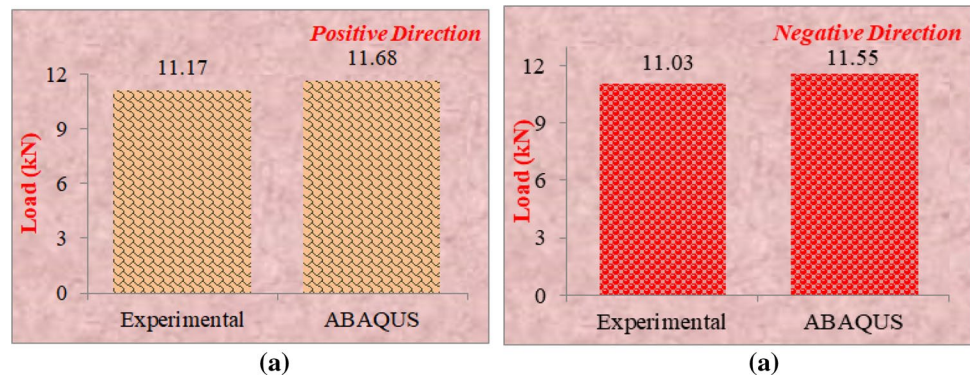


Table 5 Ductility ratio for both the experimental and ABAQUS results

S. no.	Specimen	Yield displacement (mm) Δy		Ultimate displacement (mm) Δu		Ductility factor μ		Average ductility factor
		Positive	Negative	Positive	Negative	Positive	Negative	
1	Experimental	2.22	2.35	9.79	10.92	4.41	4.65	4.53
2	ABAQUS	2.29	1.9	9.93	9.8	4.34	5.16	4.75

Table 6 Comparison of moment carrying capacity

Result	Moment (kNm)	
	Push direction	Pull direction
Experimental	4.57	4.52
ABAQUS	4.78	4.74

Ductility

Ductility is defined as the ability of the structure to undergo substantial deformation without the loss of stiffness. The ductility ratio was calculated by the ratio of ultimate displacement to yield displacement. The yield and ultimate displacement are the displacement corresponding to the 80% of ultimate load in the ascending and descending branch from the envelope curve (Tawfik et al. 2014). The ductility ratio was found to be 4.53 and 4.75 from the experimental and non-linear finite element analysis using ABAQUS (Table 5).

Ultimate moment

The moment carrying capacity at the connection was calculated by the product of ultimate load in the push and pull direction and the distance of loading from the joint region. The moment carrying capacity of this precast dowel connection was experimentally found to be 4.57 kNm and 4.52 kNm in the push and pull direction, respectively. The moment carrying capacity obtained from the experiment and the FEA are shown in Table 6. The FEA showed 4.8%

greater moment carrying capacity when compared with the experimental results.

Theoretical study

The shear transfer along the interface plays a critical part in the seismic response of precast structures. The shear transfer mechanism was mainly due to the effect of friction, cohesion, and dowel action when the concrete cast at different times (Papanikolaou and Thermou 2015). The shear stress at the concrete–concrete interface times was defined by various codes (Eqs 1 and 2).

1. Model code 2010 (Fib 2012)

$$\tau_{rd} = c_r \cdot f_c^{1/3} + \mu \cdot (\sigma_n + k_1 \cdot \rho \cdot f_y) + k_2 \cdot \rho \cdot \sqrt{(f_y)(f_c)} \leq \beta_c \cdot v \cdot f_c \tag{1}$$

where, C_r is the coefficient of aggregate interlock effects at rough surface, f_c is the concrete compressive strength, μ is the friction coefficient, σ_n is the compressive stress resulting from normal force acting on the interface, f_y is the yield strength of the reinforcing bars crossing the interface, k_1 is the interaction coefficient for tensile force activated in the dowels, k_2 is the interaction coefficient for flexural resistance, ρ is the reinforcement ratio crossing the interface, α is the inclination of reinforcement crossing the interface, β_c is the coefficient for the strength of the compression strut

Table 7 Parameters for calculating shear stress

C_r	f_c (N/mm ²)	μ	σ_n (N/mm ²)	K_1	K_2	ρ	f_y (N/mm ²)	β_c	ν
0.1	31.36	0.7	3	0.5	0.9	0.0028	500	0.5	0.54

Table 8 Shear force and stress at the joint region

Description	Experimental	ABAQUS	Model code 2010
Shear stress at the joint (N/mm ²)	2.89	3.02	3.09
Shear force at the joint (kN)	138.75	145.25	148.32

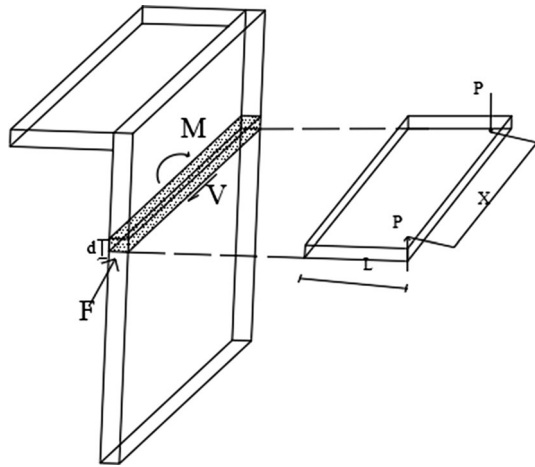


Fig. 10 Equilibrium of forces acting at the joint region

$$\nu = 0.55 \left(\frac{30}{f_{ck}} \right)^{1/3} < 0.55$$

2. Greek Code for Interventions (EPPO 2013)

$$\tau_{rd} = \beta_F \cdot \mu \cdot [f_c^2(\sigma_c + \rho f_y)]^{1/3} + \beta_D \cdot \rho \cdot \sqrt{f_y f_c} \leq 0.3 \cdot f_c \tag{2}$$

The joint shear strength of the interface can be calculated by the Eq. (3) (Table 7).

$$V = \tau_{rd} \cdot A \tag{3}$$

In this study, the shear stress, τ_{rd} and the shear force, V at the interface were calculated using the model code 2010 and compared with test results as shown in Table 8. The parameters used for obtaining the shear stress for rough interface as per model code 2010 are tabulated in Table 7.

In the shear wall to slab connection, the shear force transferred at the interface was due to the compression and tension of couple of forces from the slab when subjected to reverse cyclic loading. The shear force at the joint region was calculated from the Eq. (4) (Fig. 10). To protect the joint core from diagonal cracking, it is necessary to limit the magnitude of the horizontal joint shear stress. The shear

Table 9 Maximum joint shear stress in various codes

S. no.	Codes	Formula	Maximum joint shear stress (N/mm ²)
1	IS 13920-2016	$1.0 \sqrt{f_c k}$	6.26
2	ACI 318-02 (2002)	$K \sqrt{f_c'}$	7.00
3	NZS 3103-2006	$0.2 f_c'$	6.27

stress was also found to be within the prescribed maximum limits given by the various codes as shown in Table 9.

Shear force at the joint,

$$V = \frac{M}{d} \tag{4}$$

where M is the moment acting at the joint region (N/mm) ($M = PX$ from Fig. 10), d is the depth of the slab (mm).

Conclusion

This study aimed at developing a new ductile precast dowel connection between the exterior precast shear wall–slab and numerical model for predicting the structural performance of precast dowel connection. The reverse cyclic loading test of one-third of the scaled down precast specimen was conducted experimentally and numerically, and based on it, the following conclusions have been drawn.

- The precast specimen was loaded up to a 20 mm displacement. The load–displacement curve obtained from the experimental results showed wider hysteric behaviour and also good pinching effect due to the predefined gap between the connections.
- The ultimate strength of this dowel connection was found to be 11.17 kN and 11.03 kN in the push and pull direction, respectively.
- The ultimate moment carrying capacity of this dowel connection was obtained as 4.57 kNm and 4.52 kNm in the push and pull direction, respectively.

- The ductility ratio was found to be 4.53 which proved that the detailing of dowel connection provided between the precast shear wall and the slab showed satisfactory performance in the post-elastic stage.
- The numerical model developed showed a good correlation with the experimental results (less than 5%) which was acceptable and exactly predicted the similar structural behaviour of precast connection when subjected to reverse cyclic loading. It also showed that the damage parameter and the interaction between the precast components should be properly defined to predict the structural performance of the precast specimen.
- The shear resistance offered by the dowel connection at the joint region from the experimental and FEA results were within the limit prescribed by the various codes of practice such as IS 13920-2016, ACI 318-02 (2002) and NZS 3103-2006.

Acknowledgements This research work was supported by the Council of Scientific & Industrial Research (CSIR), New Delhi, India. The authors are thankful to the funding agency for their support.

Funding The financial assistance was provided by the Council of Scientific and Industrial Research (CSIR)-SRF to the author Ms. S. Arthi. CSIR Award Letter Number: 09/468/0494/2016 EMR-I dated 30/3/17.

Compliance with ethical standards

Conflict of interest On behalf of all authors, the corresponding author states that there is no conflict of interest.

References

- ABAQUS. (2012). *Analysis User's Manual*. Version 6.12, Dassault Systemes Simulia, Inc.
- ACI Committee 318. (2002). *Building code requirements for structural concrete (ACI 318-02) and commentary (ACI 318R-02)* (p. 439). Michigan: American Concrete Institute.
- Alfarah, B., Lopez-Almansa, F., & Oller, S. (2017). New methodology for calculating damage variables evolution in plastic damage model for RC structures. *Engineering Structures*, *132*, 70–86. <https://doi.org/10.1016/j.engstruct.2016.11.022>.
- Beilic, D., Casotto, C., Nascimbene, R., Cicola, D., & Rodrigues, D. (2017). Seismic fragility curves of single storey RC precast structures by comparing different Italian codes. *Earthquake and Structures*, *12*(3), 359–374.
- Belleri, A., Brunesi, E., Nascimbene, R., Pagani, M., & Riva, P. (2015a). Seismic performance of precast industrial facilities following major earthquakes in the Italian territory. *Journal of Performance of Constructed Facilities*, *29*(5), 04014135.
- Belleri, A., Torquati, M., Riva, P., & Nascimbene, R. (2015b). Vulnerability assessment and retrofit solutions of precast industrial structures. *Earthquake and Structures*, *8*(3), 801–820.
- Belleri, A., Marini, A., Riva, P., & Nascimbene, R. (2017). Dissipating and re-centring devices for portal-frame precast structures. *Engineering Structures*, *150*, 736–745.
- Brunesi, E., Nascimbene, R., Bolognini, D., & Bellotti, D. (2015). Experimental investigation of the cyclic response of reinforced precast concrete framed structures. *PCI Journal*, *60*(2), 57–79.
- Brunesi, E., & Nascimbene, R. (2017). Experimental and numerical investigation of the seismic response of precast wall connections. *Bulletin of Earthquake Engineering*, *15*(12), 5511–5550.
- Brunesi, E., Peloso, S., Pinho, R., & Nascimbene, R. (2018). Cyclic testing of a full-scale two-storey reinforced precast concrete wall-slab-wall structure. *Bulletin of Earthquake Engineering*, *16*(11), 5309–5339.
- Casotto, C., Silva, V., Crowley, H., Nascimbene, R., & Pinho, R. (2015). Seismic fragility of Italian RC precast industrial structures. *Engineering Structures*, *94*, 122–136.
- Dere, Y., & Koroglu, M. A. (2017). Nonlinear FE modeling of reinforced concrete. *International Journal of Structural and Civil Engineering Research*, *6*(1), 71–74. <https://doi.org/10.18178/ijscer.6.1.71-74>.
- EPPO [Earthquake Planning and Protection Organization], Greek Code for Interventions (KANEPE), Athens, 2013.
- Elliot, K.S. (2017). *Precast concrete structure*, 2nd edn. CRC Press, Taylor & Francis, New York.
- Ercolino, M., Bellotti, D., Magliulo, G., & Nascimbene, R. (2018). Vulnerability analysis of industrial RC precast buildings designed according to modern seismic codes. *Engineering Structures*, *158*, 67–78.
- FIB [International Federation for Structural Concrete], Model Code 2010 Vol. 2, Bulletin No. 66, 2012.
- IS 456:2000, Indian Standard Plain and Reinforced Concrete Code of practice. Bureau of Indian Standards. New Delhi, India 2000.
- IS 13920: Indian Standard Ductile Detailing of Reinforced Concrete Structures Subjected to Seismic forces. Bureau of Indian Standards. New Delhi, India, 1993.
- Kremmyda, G.D., Fahjan, Y.M., Psycharis, I.N. (2013). Analytical prediction of the shear resistance of precast RC pinned beam-to-column connections. In *4th ECCOMAS thematic conference on computational methods in structural dynamics and earthquake engineering*, Kos Island, Greece. <https://doi.org/10.7712/12011.3.4611.C1443>.
- Magliulo, G., Ercolino, M., Cimmino, M., Capozzi, V., Manfredi, G. (2014). Seismic behavior of beam-to-column dowel connections: numerical analysis vs experimental test. In *Second European conference on earthquake engineering and seismology*, Istanbul
- Mohammad, M.E., Ibrahim, I.S. (2015). Interface shear strength of concrete-to-concrete bond with and without projecting steel reinforcement. *Jurnal Teknologi (Sciences & Engineering)*, *75*(1), 169–172. <https://doi.org/10.11113/jt.v75.3707>
- Mohammad, M.E., Ibrahim, I.S., Abdullah, R. (2015). Finite element modelling of interface shear strength at concrete-to-concrete bond. In *Proceedings of the APSEC & ACEC*
- Mousavi, S. A., Zahrai, S. M., & Bahrami-Rad, A. (2014). A Quasi-static cyclic tests on super-lightweight EPS concrete shear walls. *Engineering Structures*, *64*, 62–75. <https://doi.org/10.1016/j.engstruct.2014.02.003>.
- Nascimbene, R. (2014). Towards non-standard numerical modeling of thin-shell structures: geometrically linear formulation. *International Journal of Computational Methods in Engineering Science and Mechanics*, *15*(2), 126–141.
- Obaidat, Y. T., Heyden, S., & Dahlblom, O. (2010). The effect of CFRP and CFRP/concrete interface models when modelling retrofitted RC beams with FEM. *Composite Structures*, *92*, 1391–1398. <https://doi.org/10.1016/j.compstruct.2009.11.008>.
- Papanikolaou, V.K., Thermou, G.E. (2015). Concrete-to-concrete interfaces under cyclic loading—Finite element analysis towards experimental verification. In *5th ECCOMAS thematic conference on computational methods in structural dynamics and earthquake*

- engineering* (pp. 666–679). Crete Island, Greece. <https://doi.org/10.7712/120115.3421.1399>.
- Rahman, A.B., Leong, D.C.P., Saim, A.A., Osman, M.H. (2006). Hybrid beam-to-column connections for precast concrete frames. In *Proceedings of the 6th Asia-Pacific Structural Engineering and Construction Conference, Kuala Lumpur, Malaysia*.
- Soudki, K. A., West, J. S., Rizkalla, S. H., & Blackett, B. (1996). Horizontal connections for precast concrete shear wall panels under cyclic shear loading. *PCI Journal*, 41, 64–80.
- Surumi, R. S., Jaya, K. P., & Greeshma, S. (2015). Modelling and assessment of shear wall–flat slab joint region in tall structures. *Arabian Journal for Science and Engineering*, 40, 2201–2217. <https://doi.org/10.1007/s13369-015-1720-z>.
- Taheri, H., Hejazi, F., Vaghei, R., Jaafar, M. S., & Aabang Ali, A. A. (2016). New precast wall connection subjected to rotational loading. *Periodica Polytechnica Civil Engineering*, 60(4), 547–560. <https://doi.org/10.3311/PPci.8545>.
- Tawfik, A. S., Badr, M. R., & Eizanaty, A. (2014). Behavior and ductility of high strength reinforced concrete frames. *Housing and Building National Research Center, HBRC Journal*, 10(2), 215–221. <https://doi.org/10.1016/j.hbrj.2013.11.005>.
- Wan, S., Loh, C. H., & Peng, S. Y. (2001). Experimental and theoretical study on softening and pinching effects of bridge column. *Soil Dynamics and Earthquake Engineering*, 21, 75–81. [https://doi.org/10.1016/S0267-7261\(00\)00073-7](https://doi.org/10.1016/S0267-7261(00)00073-7).
- Yuksel, E., Karadogan, H. F., Bal, I. E., Ilki, A., Bal, A., & Inci, P. (2015). Seismic behavior of two exterior beam–column connections made of normal-strength concrete developed for precast construction. *Engineering Structures*, 99, 157–172. <https://doi.org/10.1016/j.engstruct.2015.04.044>.
- Zoubek, B., Fischinger, M., Isakovic, T. (2016). Seismic response of dowel connections in RC structures. In *NZSEE Conference*. Christchurch, New Zealand.
- Zoubek, B., Fahjan, Y., Fischinger, M., Isaković, T. (2014). Nonlinear finite element modelling of centric dowel connections in precast buildings. *Computers and Concrete*, 14, 463–447. 10.12989/cac.2014.14.4.463.

Publisher's Note Springer Nature remains neutral with regard to jurisdictional claims in published maps and institutional affiliations.